

IEEE CGNCC 2014

August 8-10, 2014, Yantai, China

Program Digest



<http://cgnc.buaa.edu.cn>



<i>Situation for Dynamic Inverse Control Law</i>		Chair: Junsheng You	Air Force Institute of Aeromedicine
Sen Yang	Flight Automatic Control Research Institute	Haijun Zhou	Xi'an Flight Automatic Control
Xianglun Zhang	Flight Automatic Control Research Institute		Research Institute
14:00-14:15	SatA6.3	13:30-13:45	SatA7.1
<i>Compound Angle-Synchronizing Control Strategy for Dual Electro- Hydraulic Motors in HydraulicFlight Motion Simulator</i>		<i>Research on Modeling of Morphing Aircraft</i>	
Wenhao Dong	Beihang Univ.	Bowen Li	Xi'an Flight Automatic Control Research Institute
Songshan Han	Beihang Univ.	Haijun Zhou	Xi'an Flight Automatic Control Research Institute
Zongxia Jiao	Beihang Univ.	Xianglun Zhang	Xi'an Flight Automatic Control Research Institute
Shuai Wu	Beihang Univ.	Jun Che	Xi'an Flight Automatic Control Research Institute
Yifei Zhao	Beihang Univ.	Kepu Song	Xi'an Flight Automatic Control Research Institute
14:15-14:30	SatA6.4	13:45-14:00	SatA7.2
<i>Adaptive Robust H^∞ Control for Uncertain Discrete-Time Systems with Time-Varying State and Input Delays</i>		<i>Modeling and Modal Responses Analysis of an Unmanned Small-Scaled Gyroplane</i>	
Cunwu Han	North China University of Technology	Changle Xiang	Beijing Institute of Technology
Fengmei Zhang	North China University of Technology	Xiaoliang Wang	Beijing Institute of Technology
Lei Liu	North China University of Technology	Yue Ma	Beijing Institute of Technology
Song Bi	North China University of Technology	Yang Wang	Beijing Institute of Technology
Dehui Sun	North China University of Technology	14:00-14:15	SatA7.3
14:30-14:45	SatA6.5	<i>An Optimization Method of Aircraft Periodic Inspection and Maintenance Based on the Zero-Failure Data Analysis</i>	
<i>Internal Model Tracking Control of an Uncertain Impulsive Switched System</i>		Jun Huang	Naval Aeronautical and Astronautical Univ.
Jian Chen	Beihang Univ.	Yanbo Song	Naval Aeronautical and Astronautical Univ.
Chen Bai	Beihang Univ.	Yongji Ren	Naval Aeronautical and Astronautical Univ.
Qingdong Li	Beihang Univ.	Qingwei Gao	Naval Aeronautical and Astronautical Univ.
Cunjia Liu	Loughborough Univ.	14:15-14:30	SatA7.4
Yuan Tian	Beijing Institute of Space Long March Vehicle	<i>Background Modeling in Infrared Guidance Hardware-in-loop Simulation System</i>	
Zhang Ren	Beihang Univ.	Haowen Zhang	Beihang Univ.
14:45-15:00	SatA6.6	Wulong Zhang	Beijing Simulation Center
<i>Observer-based Control of One-sided Lipschitz Nonlinear Systems</i>		Yunjie Wu	Beihang Univ.
Rui Wu	Shanghai University of Engineering Science	Jianmin Wang	Beihang Univ.
Wei Zhang	Shanghai University of Engineering Science	14:30-14:45	SatA7.5
Jian Li	Shanghai University of Engineering Science	<i>Research on Boundary Layer Ingestion Effects of Distributed Propulsion Configuration</i>	
Zhiyang Wu	Shanghai University of Engineering Science	Wenwen Kang	Beihang Univ.
15:00-15:15	SatA6.7	Jing Zhang	Beihang Univ.
<i>Robust Attitude Control for Flexible Satellite During Orbit Maneuver</i>		Lingyu Yang	Beihang Univ.
Long Li	Harbin Institute of Technology	14:45-15:00	SatA7.6
Jing Yang	Harbin Institute of Technology	<i>Research on Supercirculation Effects of Distributed Propulsion Configuration</i>	
Xiaoping Shi	Harbin Institute of Technology	Wenwen Kang	Beihang Univ.
Hailong Liu	Harbin Institute of Technology	Jing Zhang	Beihang Univ.
15:15-15:30	SatA6.8	Lingyu Yang	Beihang Univ.
<i>Dynamic Control Algorithm Design of the 6 Wheel-drive All-terrain Robotic Skid-steered Vehicles</i>		15:00-15:15	SatA7.7
Tong Liu	Luoyang Institute of Electro-Optical Equipment, AVIC	<i>An HLA/RTI Architecture Based on Periodic and Aperiodic Tasks Scheduling for Real-time Improvement</i>	
Wei Li	Luoyang Institute of Electro-Optical Equipment, AVIC	Shutian Liu	Beihang Univ.
Beile Wang	Luoyang Institute of Electro-Optical Equipment, AVIC	Shuling Dai	Beihang Univ.
Yuqian Li	Luoyang Institute of Electro-Optical Equipment, AVIC	15:15-15:30	SatA7.8
SatA7		<i>A Real-Time Flight Simulation System Based on Rapid Prototyping and VxWorks</i>	
Modeling & Simulation I (Regular Session)		Xintao Liao	Nanjing Univ. of Aeronautics and Astronautics
APPHIRE			

Research on Boundary Layer Ingestion Effects of Distributed Propulsion Configuration

Wenwen Kang, Jing Zhang, Lingyu Yang

Abstract—Boundary Layer Ingestion (BLI) effects are the new and special issues caused by the in-depth integration of airframe and propulsion system. Based on a mathematical model of the distributed propulsion system and a sliced CFD model of SAX-40, this paper presents a detailed numerical research on the BLI effects of distributed propulsion configuration. The influence regularities of BLI on aerodynamic parameters are summarized and analyzed. Computation results indicate that BLI has extraordinary potential to raise the CI and L/D ratio, thus resulting in a better flight performance.

I. INTRODUCTION

To achieve the target of Greener Aviation, the next generation of large civil aircraft is faced with highly demanding requirements on many aspects such as pollution emission and noise. NASA has proposed an “N+X” program ^[1], i.e. a program focused on large transport aircraft whose technologies are ahead of current situation with X generations. The mainly demonstrated configuration named “N+3” is shown as Figure 1.



Figure 1 “N+3” configuration

Cambridge University (CM) and MIT have also carried out a SAI (Silent Aircraft Initiative) program ^[2], and their design output is called SAX-40, shown as Figure 2.



Figure 2 SAX-40 configuration

*Resrach supported by National Natural Science Foundation of China with Grant No. 61304030.

F. A. Wenwen Kang is with the Science and Technology on Aircraft Control Laboratory, Beihang University, Beijing, 100191 China (e-mail: wanderkang0530@163.com).

S. B. Jing Zhang and S.C. Lingyu Yang are with School of Automation Science and Electrical Engineering, Beihang University, Beijing, 100191 China.(e-mail: jijzhj1982@163.com).

The distributed propulsion system (DPS) of SAX-40 consists of three separate engines, while the N+3 configuration is more advanced whose DPS covers 2/3 of the wing span. The two hotly demonstrated configurations imply that the next generation of large aircraft is most likely to select the integration of BWB (Blended Wing Body) layout and DPS, namely distributed propulsion configuration (DPC).

DPC is a new integrated design of civil aircraft. With the distributed thrust along the rear edge, it can absolutely reduce pollution emission and noise, and enhance fuel economy and range. Compared to the traditional BWB aircraft, the most important innovation of DPC is the application of a semi-embedded DPS which features the function of Boundary Layer Ingestion. By ingesting the boundary layer flow of the upper fuselage surface into engine inlets, BLI can significantly improve the aerodynamic performance.

Current research on BLI can be divided into three main categories ^{[3]-[8]}: (1) the basic characteristics of BLI and its influence on the engine performance; (2) inlet and nacelle design featuring BLI; (3) active flow control in the inlet. These studies only concern about the internal influence of engine, while the impact of BLI on the aerodynamic characteristics is not discussed, which the main topic of this paper is.

To study the impact of BLI on aerodynamic characteristics, SAX-40 from CM and MIT is chosen as the research object, and CFD (Computational Fluid Dynamics) analysis methods are applied.

To simulate BLI in CFD effectively and with high fidelity, a mathematical model of DPS and a set of CFD models of SAX-40 are established firstly; then simulation of BLI under different conditions is carried out; finally the influence regularities of BLI on aerodynamic characteristics are summarized. The DPS model can provide inlet/outlet parameters of engine for CFD model as boundary conditions, and provide other propulsion system states such as thrust and power etc. Simulation results of CFD model will be used to modify the DPS model, and support the analysis of BLI effects.

II. DEFINITION OF BLI

DPS is usually installed semi-embedded on the upper rear edge of BWB fuselage, leading to the typical characteristic BLI. The initiative purpose of BLI is to suck the wake flow on the upper surface into engine, resulting in a better fuel economy. Illustration of BLI is shown as Figure 3.

III. MODELING AND SIMULATION OF DPS

The purpose of building a DPS mathematical model is to provide boundary conditions for the CFD model, and to calculate engine states data such as thrust. The DPS of SAX-40 consists of three sets of engines, and the adjustable parameters of each set are independent. The structure of SAX-40's DPS is shown as Figure 5.

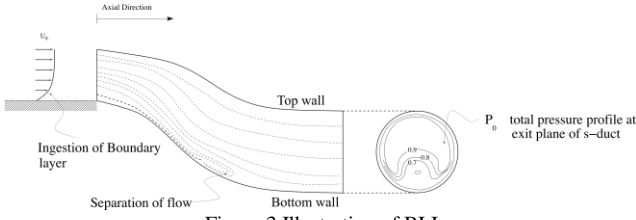


Figure 3 Illustration of BLI

Definition of BLI intensity in this paper is “ratio of areas which refers to a cross-section in the far field perpendicular to flight velocity tagged with A_0 and a cross-section of engine inlet tagged with A_{01} whose air mass flow rate are the same”, illustrated as Figure 4.

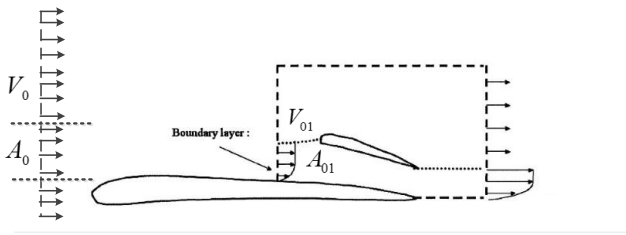


Figure 4 Definition of BLI intensity

Air mass flow rate A_{01} is defined as (calculated by):

$$q_m = K \frac{P_{01}^* * A_{01} * q(\lambda_{01})}{\sqrt{T_{01}^*}}$$

Similarly, Air mass flow rate A_0 is:

$$q_m = K \frac{P_0^* * A_0 * q(\lambda_0)}{\sqrt{T_0^*}}$$

According to the model characteristics of DPS, we have:

$$P_{01}^* = P_0^*, T_{01}^* = T_0^*$$

Then the intensity of BLI can be defined as:

$$\eta_{BLI} = \frac{A_0}{A_{01}} = \frac{q(\lambda_{01})}{q(\lambda_0)}$$

Note this, flow function $q(\lambda)$ is defined as:

$$q(\lambda) = \left(\frac{\gamma+1}{2} \right)^{\frac{1}{\gamma-1}} \lambda \left(1 - \frac{\gamma-1}{\gamma+1} \lambda^2 \right)^{\frac{1}{\gamma-1}}$$

In this equation, λ is the velocity coefficient and it is constrained with equation as below

$$\lambda^2 = \frac{\frac{\gamma+1}{2} Ma^2}{1 + \frac{\gamma-1}{2} Ma^2}$$

Where γ is the specific heat ratio, and Ma is Mach number. To express conveniently, symbol “BLI” is sometimes used instead of η_{BLI} .

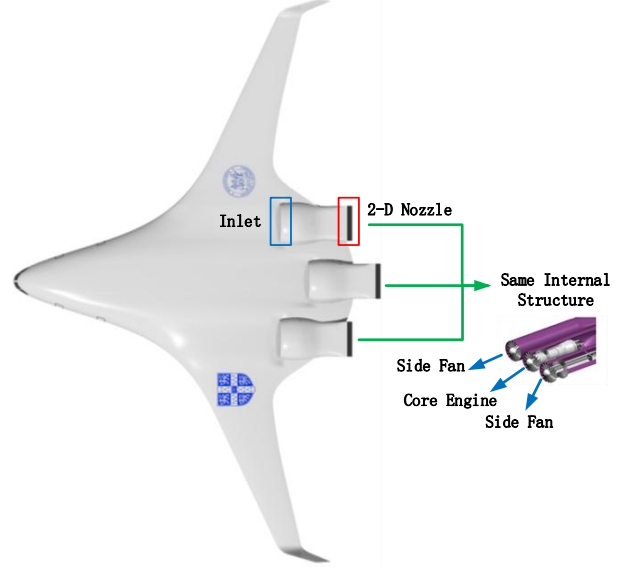


Figure 5 The DPS of SAX-40

Each set of engine is combined with three separate fans, which are located in three separated tunnels, but the inlet and nozzle are common; the core engine is in the middle tunnel, and provides power to all three fans by gear mechanism.

To Simplify the DPS model, three assumptions are taken into consideration:

- 1) The thrust of DPS is mainly generated by three fans, and the core engine is mainly used to provide power;
- 2) The impact of BLI on the engine is not considered, and the performance of three fans are assumed to be ideal, which means the rotation velocity and flow rate characteristic are not taken into consideration;
- 3) Due to the common inlet and nozzle of three tunnels, each fan of separated engine feels the same environment, thus the thermodynamic and gas dynamic parameters at inlet and outlet are the same as each tunnel.

One of the three sets of Simplified DPS model is shown as Figure 6.

The DPS model has three sets of engines or nine tunnels in total, and each tunnel has the same structure, thus only one tunnel is modeled. The detailed modeling process is shown as below:

A. Explanation of air conditions

Given the Mach number and altitude, the static pressure, static temperature, flight velocity P_0, T_0, V_0 and total pressure (i.e. stagnation pressure), total temperature, sound velocity, Mach number P_0^*, T_0^*, a_0, Ma_0 can be obtained.

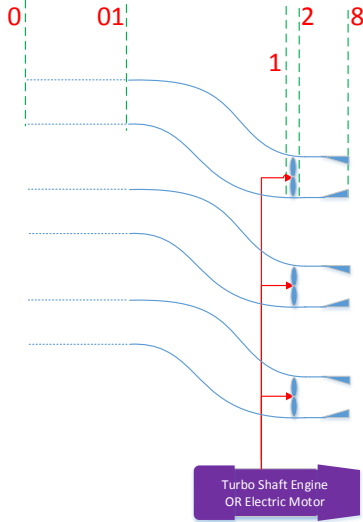


Figure 6 Illustration of DPS model

Explanations of section number: “0” represents the entrance of selected control body, which is located in the undisturbed airflow far ahead; “01” represents the entrance of inlet; “1” represents the front section of fan; “2” represents the rear section of fan; “8” represents the exit of nozzle; area between “0” section and “01” section is called pre-compression segment; inlet is located between “01” section and “1” section; fan is located between “1” section and “2” section; nozzle is located between “2” section and “8” section.

The model is built according to the principle of constant specific heat, and the constant specific heat ratio is $\gamma = 1.4$; the gas constant of air is $R = 287.06(kg * K)$. Some important parameters can be described as functions of γ and R , shown as below:

1) the specific heat at constant pressure is $Cp = \frac{\gamma}{\gamma - 1} R$;

2) the coefficient of flow function is $K = \sqrt{\frac{\gamma}{R} \left(\frac{2}{\gamma + 1} \right)^{\frac{\gamma + 1}{\gamma - 1}}}$;

3) the critical pressure ratio of nozzle is

$$\beta_{cr} = \frac{P_{ecr}}{P_e^*} = \left(\frac{2}{\gamma + 1} \right)^{\frac{\gamma}{\gamma + 1}};$$

4) the sound velocity of each point in the flow field is $a = \sqrt{\gamma RT}$.

B. Modeling of engine components

The thermodynamic process of each component is assumed as: (1) the pre-compression segment has an adiabatic process, which means the total temperature T^* and total pressure P^* in this segment are invariant; (2) the inlet also has an adiabatic process, but there is loss in total pressure, and the total pressure recovery coefficient σ_i is assumed as a constant; (3) the fan is a main power-consuming component in

each tunnel, and its pressure ratio π_k^* is an adjustable parameter; (4) the nozzle is a convergent tube, and it has an adiabatic process. The area of its exit A_8 can be adjusted. Similarly there is a loss in total pressure σ_e .

Adjustable parameters of each tunnel include fan pressure ratio π_k^* and nozzle outlet area A_8 .

Based on the above assumption of thermodynamic process of each component, characteristic equations can be summarized as below:

1) Pre-compression segment, $P_{01}^* = P_0^*, T_{01}^* = T_0^*$;

2) Inlet, $P_1^* = \sigma_i^* P_{01}^*, T_1^* = T_{01}^*$;

3) Fan, $P_2^* = \pi_k^* P_1^*, T_2^* = T_1^* (\pi_k^*)^{\frac{\gamma - 1}{\gamma}}$;

4) Nozzle, $P_8^* = \sigma_e^* P_2^*, T_8^* = T_2^*$.

C. Balance of air mass flow rate at each section

The air mass flow rates at the inlet and outlet of each tunnel are the same, which can be described as:

$$q_m = K \frac{P_{01}^* A_{01}^* q(\lambda_{01})}{\sqrt{T_{01}^*}} = K \frac{P_8^* A_8^* q(\lambda_8)}{\sqrt{T_8^*}} \quad (1)$$

Using the characteristic equations of components, equation as below can be deduced:

$$q(\lambda_{01}) = \sigma_i^* (\pi_k^*)^{\frac{\gamma + 1}{2\gamma}} A_8^* q(\lambda_8) / A_{01} \quad (2)$$

D. Supplementary equations

Because A_8 is a critical section, the air condition at this section must be analyzed to determine whether the compressed air in the nozzle is fully expanded.

Total pressure P^* and static pressure P in the flow field has relationship as:

$$\frac{P^*}{P} = \left(1 + \frac{\gamma - 1}{2} Ma^2 \right)^{\frac{\gamma}{\gamma - 1}} \quad (3)$$

Total pressure T^* and static pressure T in the flow field has relationship as:

$$\frac{T^*}{T} = 1 + \frac{\gamma - 1}{2} Ma^2 \quad (4)$$

E. Thrust and power

The air velocity at A_8 is $V_8 = Ma_8^* a_8 = Ma_8^* \sqrt{\gamma RT_8^*}$, therefore the thrust of each tunnel is:

$$F = q_m^* (V_8 - V_0) + A_8^* (P_8 - P_0) \quad (5)$$

And the power-consumed of each tunnel is:

$$P_{re} = q_m^* w_k \quad (6)$$

Where w_k is the power consumed by unit air mass flow rate, and it can be described as:

$$w_k = Cp(T_2^* - T_1^*) / \eta_k^* = \frac{\gamma}{\gamma - 1} R^* T_0^* \left[\left(\pi_k^* \right)^{\frac{\gamma - 1}{\gamma}} - 1 \right] / \eta_k^* \quad (7)$$

In which, η_k^* is the efficiency of power transmission from shaft power to compression power.

As above, all the equations needed to build a DPS mathematical model are described. If the initial conditions are set, all the thermodynamic and gas dynamic parameters at each section can be obtained.

F. Modification of DPS model and settings of adjustable parameters

To modify the design parameters of the basic DPS model, information such as required thrust must be extracted from CFD results.

When the modification has been done, the available range of adjustable parameters of DPS model should be set. There are two limit conditions:

- 1) Usable total thrust should cover all the situations which could occur during the whole cruising state, e.g. the whole range of AOA (Angle of Attack) variation;
- 2) Usable air mass flow rate should be limited to keep the Mach number of the entrance of inlet under 1, i.e. $Ma_{01} < 1$, because the inlet of SAX-40 is designed to work at subsonic condition.

G. Extract BLI intensity from DPS model

After the modeling of DPS has been completed, the intensity of BLI can be deduced as:

$$\eta_{BLI} = \frac{A_0}{A_{01}} = \frac{q(\lambda_{01})}{q(\lambda_0)} \quad (8)$$

In which, $q(\lambda_0)$ can be directly determined by flight states, and $q(\lambda_{01})$ can be obtained from DPS mathematical model.

H. Simulation of DPS model

Choosing $Ma = 0.6$, $H = 10000m$ as the initial flight states, the usable thrust of each tunnel is $12.4kN \sim 23.3kN$, then the usable total thrust of DPS model is $112kN \sim 210kN$; the usable air mass flow rate of each tunnel is $151kg/s \sim 184kg/s$ and the usable η_{BLI} is $0.96 \sim 1.19$.

To present a clear comparison, the usable thrust range and the usable air mass flow rate range are shown as Figure 7.

Some basic laws can be inferred from the simulation results of DPS model: (1) the slope of two surfaces are not consistent, which means the changing trend of usable thrust and usable air mass flow rate along with the adjustable parameters of DPS model are not in accordance; (2) from the distribution of F contours and q_m contours, it can be inferred that to obtain equal F , q_m can be changed with different

combination of adjustable parameters, and to obtain equal q_m , F can be changed, too.

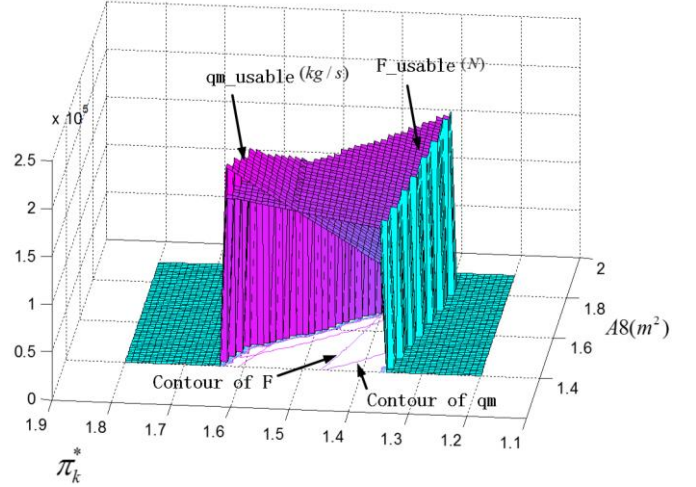


Figure 7 The usable thrust and usable air mass flow rate

IV. 2D SLICED CFD MODELING OF SAX-40

The sliced model of SAX-40 is firstly conducted to explore BLI effects on 2-Dimension. Modeling of SAX-40 consists of two main procedures:

- 1) 3D clean CFD model of SAX-40 should be established to prove the validity of SAX-40 configuration;
- 2) 2D sliced clean model should be extracted from 3D model, and the 2D model can be modified into an intact one with the integration of DPS model.

A. 3D clean model

To provide reference data for DPS modeling, 3D clean CFD model should be built firstly. The 3D shape reconstruction of SAX-40 is shown as Figure 8.

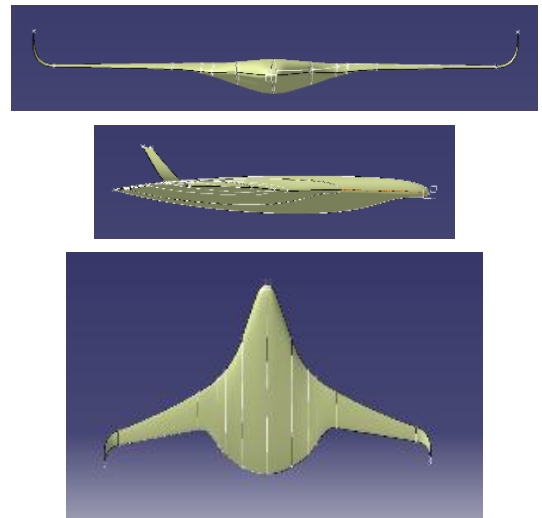


Figure 8 Reconstruction results of 3D shape

Numerical simulation results such as the Cl i.e. Cl and the drag coefficient Cd under different flight Mach numbers are shown as Figure 9.

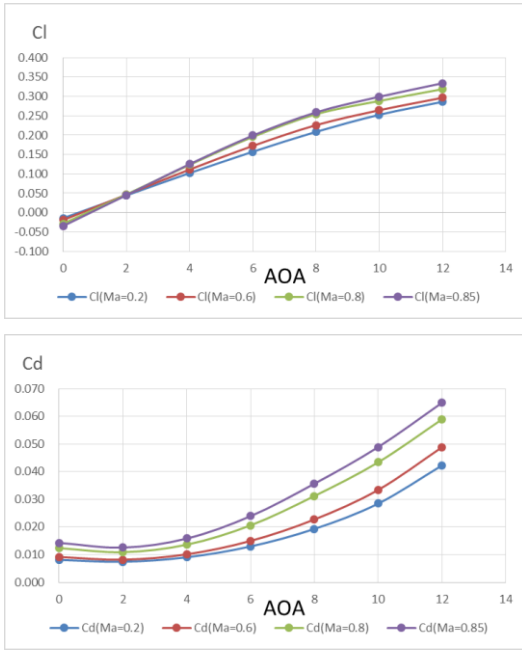


Figure 9 Aerodynamic Parameters of 3D model

As can be seen, first the Cl is linearly changing with AOA, while Cd is changing with AOA in a quadratic curve. The changing trend is in accordance with the conventional experience; secondly, through an integrated analysis with design parameters such as total cruising weight and reference area of the wing, conclusions can be made that the 3D CFD simulation results are logical and rational and SAX-40 configuration can be selected as the basis for further discussion.

B. 2D sliced clean model

BLI effects are mostly generated in front of the entrance of inlet, i.e. the upper surface of central fuselage. To simplify the analysis, the regions shown as Figure 10 in shadows are considered as the main affected regions in this article.

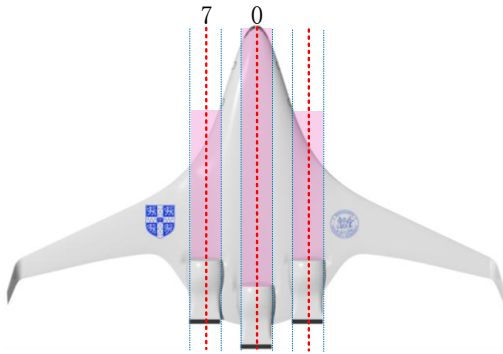


Figure 10 Regions affected by BLI

Since the 3D shape of SAX-40 has been established, 2D sliced model can be easily extracted from the corresponding position from 3D model. Taking the areas affected by BLI into consideration, the clean airfoil of “7” position are extracted, as shown as Figure 11.

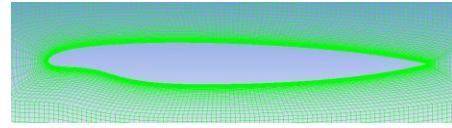


Figure 11 Sliced models of clean airfoil

The purpose of extracting 2D sliced clean model is to provide a reference to BLI effects and to provide a basic model for modifying.

C. 2D sliced model integrated with DPS model

With the specific design parameters of DPS model, the 2D clean airfoil can be modified with the shape of propulsion system, and the modified results are shown as Figure 12.

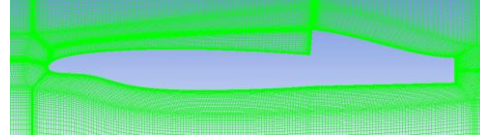


Figure 12 Sliced models with engine shape

To simulate BLI effects with CFD measures, the DPS model should be integrated into the CFD model. Correspondingly, the DPS model provides the CFD model with boundary conditions, shown as Figure 13.

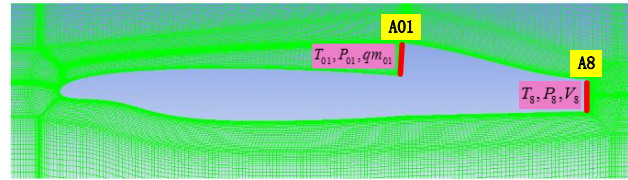


Figure 13 Illustration of required boundary conditions

V. STUDY ON INFLUENCE REGULARITIES OF BLI

In this paper, two kinds of initial flight conditions are chosen to conduct CFD simulation on BLI effects, as shown below:

- 1) $Ma = 0.6, H = 10000m, \alpha = 0^\circ$;
- 2) $Ma = 0.8, H = 10000m, \alpha = 0^\circ$.

The slice “7” is selected as the analysis area. First, the visualized nephograms will be presented to give an intuitionistic explanation; then, a systematic analysis based on the numerical data will be presented.

A. Simulation results of slice “7” under the condition of $Ma = 0.6, H = 10000m$

- 1) The velocity nephograms of slice “7” with clean airfoil and BLI effects $\eta_{BLI} = 1.08$ are shown separately as Figure 14.

As can be seen, the jet velocity of propulsion system is apparent, which is in accordance with the DPS data, and the flow velocity on the upper surface of airfoil is obviously raised with BLI.

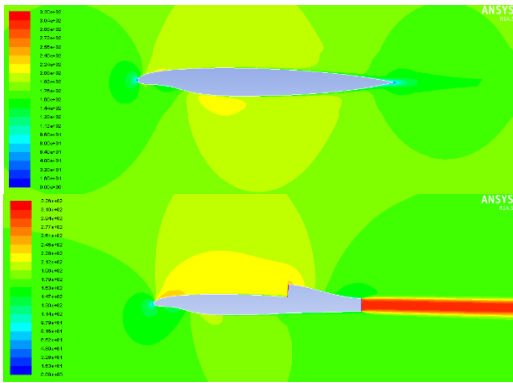


Figure 14 Comparison of velocity nephograms

- 2) The pressure nephograms of slice “7” with clean airfoil and $\eta_{BLI} = 1.08$ are shown as Figure 15.

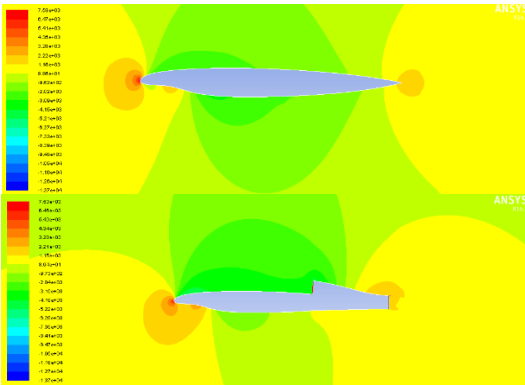


Figure 15 Comparison of pressure nephograms

As can be seen, as a result of increased velocity on the upper surface of airfoil and a renewed distribution of air mass flow rate around the airfoil, the static pressure on the upper surface decreases apparently; on the contrary, the static pressure on the under surface increases distinctly.

- 3) A systematic simulation is conducted under conditions with different parameters (π_k^* , $A8$) of the DPS model. Simulation results of aerodynamic parameters including C_l and C_d are shown as Figure 16.

Four influence regularities can be concluded from the curves:

- Under conditions of equal nozzle jet velocity, along with the deepening of BLI, the C_l increases and the C_d decreases. Thus the L/D ratio increases. These obviously agree with the phenomena reflected from the nephograms. The reasons include: (1) the increasing flow velocity on the upper surface and simultaneously decreasing velocity on the under surface alter the static pressure distribution around the airfoil; (2) on the other hand, the increasing flow velocity on the upper surface delays the occurrence of flow separation, and in consequence, decreases the frictional drag and pressure drag; (3) at the same time, the ram drag occurred at the entrance of inlet is decreased substantially with the deepening of BLI.
- Under conditions of equal BLI intensity, along with the increasing of jet velocity, the C_l decreases, and C_d first increases and then decreases. The reasons include: (1)

the Mach number is low, and when the jet velocity is relatively higher, the jet will affect the flow field around the airfoil with inducing effect. As a result of this, the flow velocity on the under surface increases and the static pressure decreases simultaneously. However, due to the impediment of semi-embedded inlet, the static pressure on the upper surface doesn't decrease apparently; (2) the increased flow velocity on the under surface reduces the frictional drag and pressure drag, but the increased flow velocity on the nacelle raises pressure drag on the upper surface. The synthesized result is just described as the nonlinearly changing of C_d .

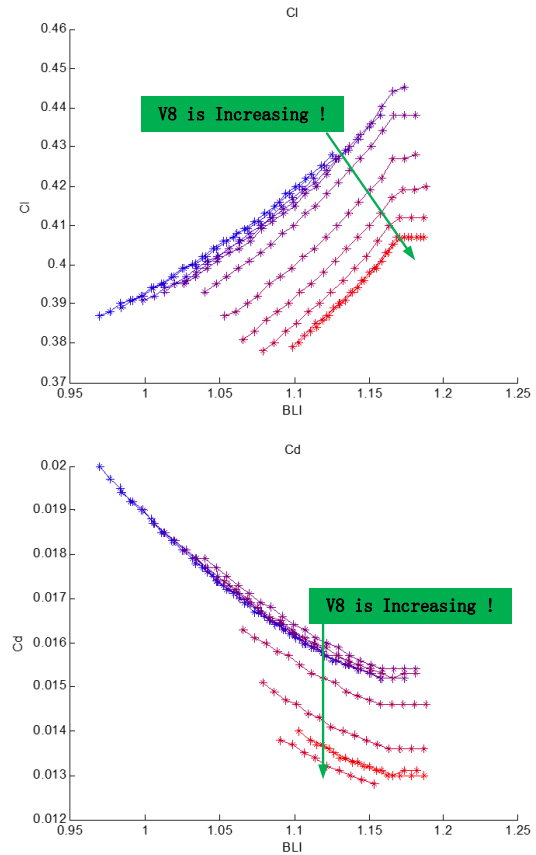


Figure 16 Aerodynamic parameters of Slice “7” with varied BLI

- When the BLI intensity raises to 1.15, there will emerge an upper limit to the lift and C_d . This phenomenon indicates that the BLI intensity cannot be raised infinitely and the flow velocity cannot go on increasing after a specific intensity of BLI. The reason is that when the BLI intensity is raised to some kind of extent, the flow velocity near the entrance of inlet will draw near to 1 Mach, and there will emerge stall phenomenon locally. This is in accordance with numerical results of DPS model.
- The aerodynamic parameters vary almost linearly along with the range of (π_k^* , $A8$) parameters of DPS model, and this will provide convenience for application of BLI effects.

The aerodynamic parameters of slice “7” with clean airfoil under conditions of $Ma = 0.6$ and $AOA = 0^\circ$ are shown as below:

$$Cl = 0.0276$$

$$Cd = 0.0153$$

$$K = 1.8$$

Three influence regularities can be concluded from numerical comparisons of the clean model and the BLI model:

- The Cl is raised apparently with BLI effects, and this indicates that the BLI effects have great potential to improve the flow field around the airfoil;
- The Cd is relatively higher with BLI effects than the clean model, but along with the increasing BLI effects, the ram drag is effectively reduced. This is consistent with actual situation, and indicates the validity of CFD models.
- The L/D ratio is raised obviously with increasing BLI effects, and this implies that the BLI effects have great potential to improve the performance of SAX-40.
- To analyze the influence of jet velocity on BLI effects in-depth, aerodynamic data under equal BLI effects is extracted from initial calculation results. The jet velocity of the nozzle $V8$ is chosen as the abscissa factor, and the results are shown as Figure 17.

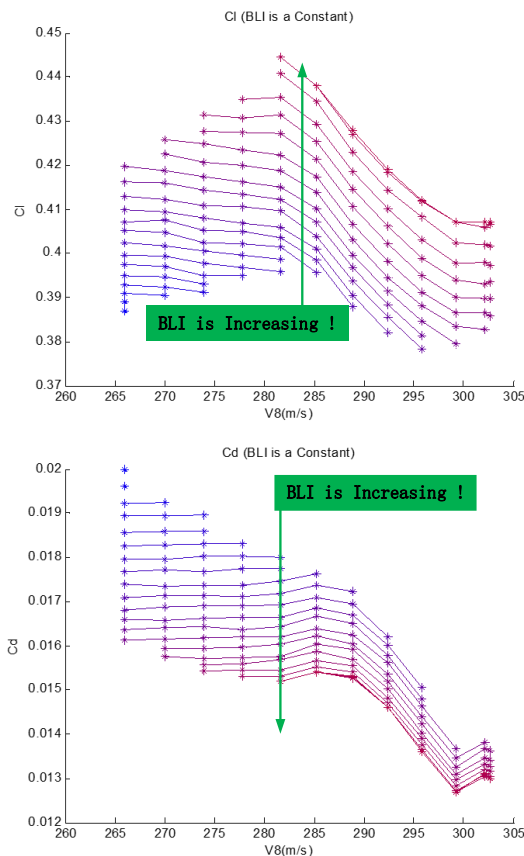


Figure 17 Aerodynamic parameters of Slice “7” with varied $V8$. Two influence regularities can be concluded from the curves:

- When $V8$ is less than 280m/s , its influence on aerodynamic parameters is negligible; but when $V8$ is large sufficiently, its influence will be more and more obvious.
- Under the equal BLI intensity, the influence of $V8$ on aerodynamic parameters appears to be nonlinear, but the variation gap between different BLI intensities is almost the same. This can be deduced from that the curves of different BLI intensities are almost parallel.
- To analyze the challenge of BLI effects on integrated flight/propulsion control, aerodynamic data under the equal thrust is extracted from initial results. π_k^* and $A8$ both are the influence factors of thrust. Choosing $A8$ as the abscissa factor, the results are shown as Figure 18.

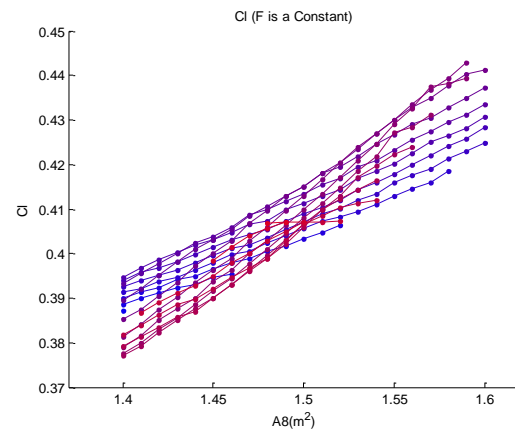


Figure 18 Aerodynamic parameters of Slice “7” with equal thrust. As can be seen, with the same thrust, change of the parameters $A8$ can alter the BLI intensity, resulting in changing of aerodynamic parameters. And when the thrust is being adjusted, the corresponding aerodynamic parameters will present a strong nonlinearity.

B. Simulation results of slice “7” under the condition of $Ma = 0.8, H = 10000\text{m}$

- Due to the relatively high Mach number, the influence of $V8$ on BLI effects needs to be discussed first. Under a same BLI intensity, the results of $V8$ influence on aerodynamic parameters are shown as Figure 19.

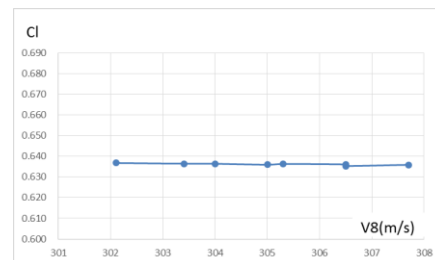


Figure 19 Influence of $V8$ on Aerodynamic parameters. As can be seen, when the Mach number is relatively high, the influence of $V8$ is little enough, which can be neglected.

- Under the different conditions of π_k^* and $A8$. Simulation results of aerodynamic parameters such as Cl , Cd are shown as Figure 20.

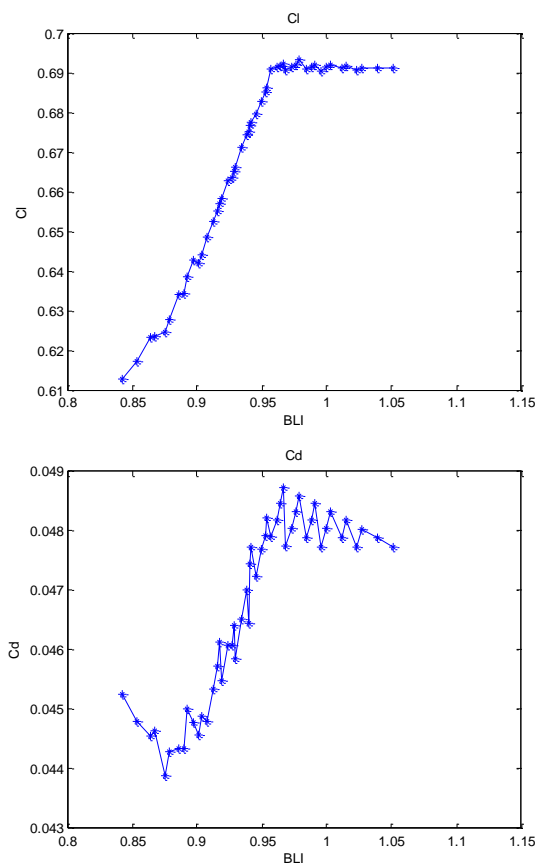


Figure 20 Aerodynamic parameters of Slice “7” with varied BLI under 0.8Ma

Aerodynamic parameters of slice “7” with clean airfoil under conditions of $Ma = 0.8$ and $AOA = 0^\circ$ are shown as below:

$$Cl = 0.0238$$

$$Cd = 0.0307$$

Four influence regularities can be concluded from the curves and numerical comparisons:

- a) The Cl increases with the deepening of BLI intensity, which is in accordance with the conditions of $Ma = 0.6$.
- b) The Cd decreases first and then increases rapidly, which appears different with the situations under $Ma = 0.6$. This is because the current Mach number is sufficiently high, and when the BLI effects is introduced, there will emerge the shock wave on the upper surface of airfoil. This will result in introducing of wave drag, and the wave drag increases with the deepening of BLI intensity. The typical pressure nephogram in this situation is shown as Figure 21.

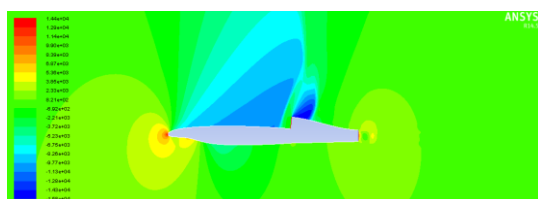


Figure 21 Pressure nephogram of shock wave

- c) There will emerge an upper limit to the change of Cl , Cd with the BLI intensifying, which is similar to the situation $Ma = 0.6$. This is in accordance with the DPS calculation results.
- d) Compared to the clean model, BLI effects can improve the Cl obviously, but with the introduction of wave drag, the Cd cannot be reduced as $Ma = 0.6$. Generally, BLI effects can raise the L/D ratio drastically, which indicates the BLI effects can improve the performance of SAX-40 at high-subsonic conditions $Ma = 0.8$.

VI. CONCLUSION

The results indicate that BLI is an important feature of DPC. The strong nonlinear influence of BLI on aerodynamic parameters poses a new challenge on integrated flight propulsion control, which requires further study.

Furthermore, systematic influence regularities based on the 2D sliced CFD model are summarized and concluded, which lay the foundation of further work and point out the future research directions on DPC.

ACKNOWLEDGMENT

Many Thanks for my adviser sincerely, who is a beautiful patient lady, and the most talented person I have ever met.

REFERENCES

- [1] Martin M. D'Angelo GE Aviation, Lynn, Massachusetts John Gallman Vicki Johnson N+3 Small Commercial Efficient and Quiet Transportation for Year 2030-2035[R] NASA/CR-2010-216691
- [2] Ann Dowling Ed Greitzer The Silent Aircraft Initiative – Overview[C] 45th AIAA Aerospace Sciences Meeting, Reno, 9th January 2007
- [3] Amer Jamal Anabtawi Experimental investigation of boundary layer ingestion into diffusing inlets[R] NASA 1999
- [4] Leroy H. Smith Jr. Wake Ingestion Propulsion Benefit[J] JOURNAL OF PROPULSION AND POWER Vol. 9, No. 1, Jan.-Feb. 1993
- [5] Angelique Plas Performance of a Boundary Layer Ingesting Propulsion System[R] NASA 2006
- [6] Patrick N. Freuler Boundary Layer Ingesting Inlet Design for a Silent Aircraft[R] NASA 2005
- [7] Byung Joon Lee and Meng-Sing Liou Chongam Kim Optimizing a Boundary-Layer-Ingestion Offset Inlet by Discrete Adjoint Approach[C] AIAA JOURNAL Vol. 48, No. 9, September 2010
- [8] Lewis R. Owens, Brian G. Allan and Susan A. Gorton Boundary-Layer-Ingesting Inlet Flow control[R] NASA 2003